A Quantum Mechanics/Molecular Mechanics Study of the Catalytic Mechanism and Product Specificity of Viral Histone Lysine Methyltransferase†

Xiaodong Zhang and Thomas C. Bruice*

Department of Chemistry and Biochemistry, University of California, Santa Barbara, California 93106

Received March 14, 2007; Revised Manuscript Received June 6, 2007

ABSTRACT: There are three reaction steps in the *S*-adenosylmethionine (AdoMet) methylation of lysine-NH_2 catalyzed by a methyltransferase. They are (i) combination of enzyme·Lys-NH_3^+ with AdoMet, (ii) substrate ionization to provide enzyme·AdoMet·Lys-NH_2, and (iii) methyl transfer providing enzyme·AdoHcy·Lys-N(Me)H_2^+ and the dissociation of AdoHcy. In this study of the viral histone methyltransferase (vSET), we find that substrate ionization of vSET·Lys27-NH_3^+, vSET·Lys27-N(Me)H_2^+, and vSET·Lys27-N(Me)$_2$H$^+$ takes place upon combination with AdoMet. The presence of a water channel allows dissociation of a proton to the solvent. There is no water channel in the absence of AdoMet. That the formation of a water channel is combined with AdoMet binding was first discovered in our investigation of Rubisco large subunit methyltransferase. Via a quantum mechanics/molecular mechanics (QM/MM) approach, the calculated free energy barrier ($\Delta G^{\ddagger}$) of the first methyl transfer reaction catalyzed by vSET [Lys27-NH_2 + AdoMet → Lys27-N(Me)H_2^+ + AdoHcy] equals 22.5 ± 4.3 kcal/mol, which is in excellent agreement with the free energy barrier (21.7 kcal/mol) calculated from the experimental rate constant (0.047 min^{-1}). The calculated $\Delta G^{\ddagger}$ of the second methyl transfer reaction [AdoMet + Lys27-N(Me)H → AdoHcy + Lys27-N(Me)$_2$H$^+$] at the QM/MM level is 22.6 ± 3.6 kcal/mol, which is in agreement with the value of 22.4 kcal/mol determined from the experimental rate constant (0.015 min^{-1}). The third methylation [Lys27-N(Me)$_2$ + AdoMet → Lys27-N(Me)$_3^+$ + AdoHcy] is associated with a $\Delta G^{\ddagger}$ of 23.1 ± 4.0 kcal/mol, which is in agreement with the value of 23.0 kcal/mol determined from the experimental rate constant (0.005 min^{-1}). Our computations establish that the first, second, and third methyl transfer steps catalyzed by vSET are linear S_N2 reactions with the bond making being ∼50% associative.

Protein lysine methyltransferases catalyze the methylation of a site-specific lysine residue by *S*-adenosylmethionine (AdoMet).[1] This covalent modification regulates numerous genomic functions, in particular, gene expressions and the structure of the packaging of DNA in eukaryotes (known as the chromatin) (*1*, *2*). The transfer of methyl from AdoMet to a lysine residue in the N-terminal histone tail catalyzed by histone lysine methyltransferases (HKMTs) is an important reaction for controlling the chromatin structure (*3*). The absence of the site-specific methyltransferase enzyme activity is the origin of human diseases, notably cancer (*4*). All but Dot1p (known as H3-K79) (*5*, *6*) of the known HKMTs are characterized by a conserved SET domain (*7*, *8*), originally identified in three *Drosophila* genes involved in epigenetic processes, which contains approximately 130 amino acid residues. Each HKMT catalyzes all or part of the reactions shown in Scheme 1 (*9*−*22*). Different numbers of the transferred methyl groups (known as product specificity) have different influences on chromatin structure and transcription (*11*).

We have described important experimental results on methyltransferases by Cheng et al. (*23*) and Trievel et al. (*24*) as well as one theoretical study (*25*) in a previous report (*26*). In a previous publication (*26*) dealing with the mechanism of rubisco large subunit methyltransferase (LSMT), it was found that the formation of a water channel occurs prior to the methylation of a lysine substrate by AdoMet. The nearly identical geometrical parameters at the transition state catalyzed by LSMT (*26*) and H3-K4 SET7/9 (*25*) suggested that they have the same mechanism, the linear S_N2 reaction.

Viral histone lysine methyltransferase (vSET) is encoded by viruses (*19*, *27*) and catalyzes the transfer of three methyl groups to the target lysine 27 of an ∼40-amino acid peptide substrate (Scheme 1). In contrast to the monomer configuration in solution for eukaryotic protein lysine methyltransferases, vSET is dimeric (*18*). In this study, we employ hybrid QM/MM and MD simulations to investigate the reaction mechanism and product specificity of the enzyme vSET. Our computations characterize the nature of the first, second, and third methyl transfer steps catalyzed by vSET and elucidate the product specificity.

MATERIALS AND METHODS

The initial structure of the vSET·AdoMet·Lys27 complex was built from the NMR structure of the vSET enzyme with *S*-adenosyl-L-homocysteine (AdoHcy) and the methylated Lys27 (MeLys) substrate [PDB entry 2G46 (*18*)]. The methyl

† This project was supported by NIH Grant 5R37DK9171-43.

* To whom correspondence should be addressed. E-mail: tcbruice@chem.ucsb.edu. Telephone: (805) 893-2044. Fax: (805) 893-2229.

[1] Abbreviations: HKMT, histone lysine methyltransferase; vSET, viral histone lysine methyltransferase; AdoMet, *S*-adenosylmethionine; AdoHcy, *S*-adenosyl-L-homocysteine; MD, molecular dynamics; QM/MM, quantum mechanics/molecular mechanics; SCCDFTB, self-consistent charge density functional tight binding; CPR, conjugate peak refinement; TS, transition state.

10.1021/bi700515q CCC: $37.00
Published on Web 08/03/2007

Scheme 1

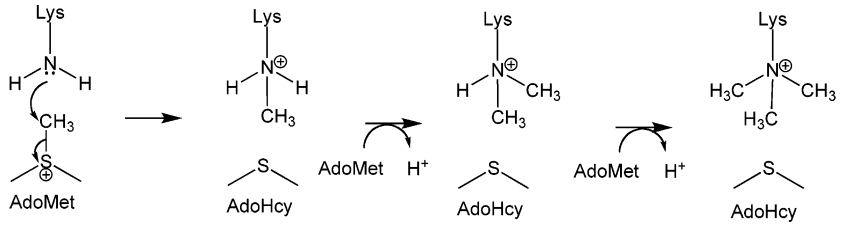

group of enzyme-bound AdoMet was built on the basis of the vSET·AdoHcy·MeLys27 structure. vSET is a dimer in the NMR structure (*18*) with 20 conformations. Ten of them are chosen as the multiple initial structures.

A water [TIP3P (*28*)] sphere with a 25 Å radius was centered at the sulfur atom of the AdoMet cofactor of each of the 10 chosen configurations. Hydrogen atoms were added to the structure using the HBUILD module implemented in CHARMM (version 31b1) (*29*), and CHARMM31 force field parameters (*30*, *31*) were employed. A spherical boundary potential (*32*) for a 25 Å radius was used to prevent the water from "evaporating" from the surface. Each complex of the 10 initial configurations, including vSET·AdoMet·Lys27-NH_3^+, vSET·AdoHcy·Lys27-NH_3^+, vSET·Lys27-NH_3^+, vSET·AdoMet·Lys27-N(Me)H_2^+, vSET·AdoHcy·Lys27-N(Me)H_2^+, vSET·Lys27-N(Me)H_2^+, and vSET·AdoMet·Lys27-N(Me)H_2^+, was minimized by the adopted basis Newton−Rasphon (ABNR) method with the threshold of the gradient 0.01 kcal mol^{-1} Å^{-1} at the MM level. Because the active site is solvated by water molecules, the sulfur atom of AdoMet was constrained with a force constant of 1.0 kcal/mol Å^{-1} during the MD simulations. Stochastic boundary molecular dynamics (SBMD) (*33*) were carried out for 4.0 ns on each complex. An integration time step of 1 fs was used, with all the bonds involving hydrogen atoms constrained using SHAKE (*34*). The water channel is characterized by the occupancies of the water molecules in the MD trajectory.

SBMD simulations were also carried out for 1.5 ns on each of 10 chosen conformations of complexes vSET·AdoMet·Lys27-NH_2, vSET·AdoMet·Lys27-N(Me)H, and vSET·AdoMet·Lys27-N(Me)$_2$. Each initial QM/MM structure was obtained by using ABNR energy minimizing the final structures of the corresponding 1.5 ns MD trajectory. QM/MM methods [QM = SCCDFTB (*35*, *36*), self-consistent charge density functional tight binding] and the threshold 0.01 kcal mol^{-1} Å^{-1} of the gradient lead to an optimized structure of the reactant. In the QM/MM calculations, the QM region included the -CH_2-S^+(Me)-CH_2- part of the AdoMet cofactor, and the side chain of the neutral target lysine 27 (Lys27-NH_2) (or neutral monomethylated lysine or neutral dimethylated lysine) of the ∼40-amino acid peptide substrate. Link atoms were introduced to saturate the valence of the QM boundary atoms.

Adiabatic mapping calculations at the SCCDFTB/MM level were carried out using a two-dimensional potential energy surface (PES). The two-dimensional reaction coordinates were the N_ϵ(Lys27)−C_γ(AdoMet) and C_γ(AdoMet)−S_δ(AdoMet) distances. The transition states were obtained using conjugate peak refinement (CPR) (*37*) implemented in the Trajectory Refinement and Kinematics module of CHARMM at the SCCDFTB/MM level, and normal-mode analysis provided only one imaginary frequency for characterizing the transition state. The Wiberg bond-order analysis (*38*) of the bond making and breaking at the SCCDFTB/MM determined transition states was carried out by use of MP2/6-31+G(d,p) [Gaussian (*39*)] in the gas phase.

Table 1: Comparison of the Structures and Wiberg Bond Orders of Bond Making and Bond Breaking at the Transition State as Well as the Potential Energy Barrier for the Monomethylation Reaction Catalyzed by Monomer SET7/9 Using SCCDFTB/MM and B3LYP/6-31G*//MM Methods

	SCCDFTB/MM	B3LYP/6-31G*//MM (25)
bond length (Å)		
S_δ(AdoMet)−C_γ(AdoMet)	2.24 ± 0.06	2.32 ± 0.01
C_γ(AdoMet)−N_ϵ(Lys4)	2.17 ± 0.04	2.30 ± 0.01
bond angle (deg)		
S_δ(AdoMet)−C_γ(AdoMet)−N_ϵ(Lys4)	172 ± 2	173 ± 1
Wiberg bond order		
S_δ(AdoMet)−C_γ(AdoMet)	0.59 ± 0.04[a]	0.58 ± 0.01
C_γ(AdoMet)−N_ϵ(Lys4)	0.33 ± 0.03[a]	0.30 ± 0.01
potential energy barrier (kcal/mol)	13.5 ± 1.7	14.6 ± 1.7

[a] Wiberg bond order analysis was carried out at the B3LYP/6-31G* level.

To validate the accuracy of the SCCDFTB/MM method, the exact same procedure of MD and QM/MM was applied on the methyl transfer reaction catalyzed by the monomeric SET7/9 enzyme [PDB entry 1O9S (*12*)]. Comparison of Table 1 with the B3LYP/6-31G*//MM calculations (*25*) indicates that SCCDFTB/MM treatment could describe the reaction coordinate of the methyl transfer reaction well. Table 2 shows that our use of SCCDFTB/MM to determine the position of the transition state followed by single-point calculation of the free energy barrier ($\Delta G^\ddagger$) with the equation $\Delta G^\ddagger = \Delta E^\ddagger + \Delta E_{ther}{}^\ddagger + \Delta(\mathrm{ZPE})^\ddagger - T\Delta S^\ddagger$ (*40*) provides a free energy of activation, which on average is approximately ±1.0 kcal/mol from the experimentally derived free energy barrier.

The potential energy (ΔE) was provided by single-point QM/MM calculations at the MP2/6-31+G(d,p)//MM level (Gamess-US, version June 22, 2002) (*45*). In this study, the activation enrgy barrier with single-point calculation at the B3LYP/6-31+G(d,p) level is ∼4.2 kcal/mol lower than the experimental values. The thermal energy (ΔE_{ther}) could be expressed as $\Delta E_{ther} = \Delta E_{trans} + \Delta E_{rot} + \Delta E_{vib}$. The vibrational contributions [Δ(ZPE), ΔE_{vib}, and $-T\Delta S$] were determined with a harmonic approximation at 298 K by normal mode analysis. Because the thermal energies and entropies from the transition motion (E_{trans}) and rotation motion (E_{rot}) are linear with temperature according to their corresponding statistical equations, their contributions to the reaction barrier (or reaction energy) should be approximately zero for an enzymatic reaction at a constant temperature.

The residues within 16 Å of AdoMet in all species [reactants, transition states, and (immediate) products] were

Table 2: Comparison of the Experimental Free Energy Barriers ($\Delta G_e^{\ddagger}$ in kilocalories per mole) and the Calculated $\Delta G_c^{\ddagger}$ by SCCDFTB/MM or the Single-Point Computations Based on the Structures Determined by SCCDFTB/MM for the Nine Reactions

$\Delta G_e^{\ddagger}$	$\Delta G_c^{\ddagger}$	$\Delta G_e^{\ddagger} - \Delta G_c^{\ddagger}$	enzyme	method	ref
21.7	22.5	−0.8	viral histone lysine methyltransferase	MP2/6-31+G(d,p)	this study
22.6	22.4	0.2	viral histone lysine methyltransferase	MP2/6-31+G(d,p)	this study
23.9	22.8	1.1	rubisco large subunit methyltransferase	MP2/6-31+G(d,p)	*26*
20.5	22.0	−1.5	rubisco large subunit methyltransferase	MP2/6-31+G(d,p)	*26*
10.3	8.3	2.0	M.Hal DNA C5 cytosine methyltransferase	SCCDFTB	*41*
10.7	8.5	2.2	quinoprotein methanol dehydrogenase	SCCDFTB	*42*
19.0	18.5	0.5	guanidinoacetate methyltransferase	B3LYP/6-31+G(d,p)	*43*
11.3	12.7	−1.4	chorismate mutase	B3LYP/6-31+G(d,p)	*44*
20.3	20.7	−0.4	chorismate in water	B3LYP/6-31+G(d,p)	*44*

Table 3: Solvent Water Molecules Forming the Water Channel and Average Occupancies of the Water Bridge during the MD Simulations

target lysine	solvent molecules forming the water channel								
	Complex: vSET·AdoMet·Lys27-NH_3^+								
	Lys27-NH_3^+	Wat914	Wat899	Wat868	Wat1315	Wat167	Wat495	Wat576	Wat832	Wat1040[b]
occupancy	0.76/0.74/0.75[a]	0.39	0.45	0.16	0.33	0.21	0.47	0.38	0.26	0.53
	Complex: vSET·AdoMet·Lys27-N(Me)H_2^+								
		Wat2114	Wat57	Wat817	Wat792	Wat984	Wat703	Wat752	Wat1970[b]	
occupancy	0.20/0.98[a]	0.59	0.15	0.22	0.10	0.11	0.51	0.10	0.27	
	Complex: vSET·AdoMet·Lys27-$N(Me)_2H^+$								
		Wat1337	Wat1239	Wat399	Wat1548	Wat671	Wat1015	Wat1290	Wat832	Wat1327[b]
occupancy	0.652[a]	0.51	0.59	0.44	0.20	0.10	0.08	0.05	0.05	0.37

[a] The average occupancies of the hydrogen bonding between the hydrogen at ϵ-amine (methylated) lysine and the oxygen of the solvent water. [b] The solvent molecule is on the surface of a water sphere with a 25 Å radius.

included in normal mode analysis to provide $3N - 6$ frequencies, which were employed to calculate the zero-point energy (ZPE), the thermal vibrational energy (E_{vib}), and the entropy ($T\Delta S$). (N is the number of atoms within the reduced regions; residues beyond that were fixed in the vibrational calculations.)

A perturbation analysis similar to that in refs *46* and *47* was performed to analyze the influence of an individual residue on the reaction barrier. Because the electrostatic contribution to the reaction barrier dominates that from van der Waals interactions, the perturbation treatment is restricted to the former. The electrostatic contribution ($\Delta\Delta E^{\ddagger}$) of a residue to the reaction barrier is defined as the difference between the potential energy barrier for a residue with no charge and that with its normal charge. Due to the extensive QM/MM calculations required, the analysis was carried out at the SCCDFTB/MM level.

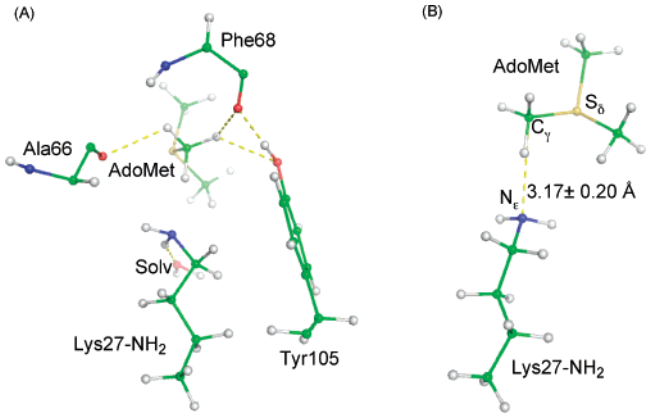

FIGURE 1: Structure of the ground state vSET·AdoMet·Lys27-NH_2 (A) and close-up of the QM region (B) in the first methyl transfer reaction vSET·AdoMet·Lys27-NH_2 → vSET·AdoHcy·Lys27-N(Me)H_2^+.

RESULTS AND DISCUSSION

The First Methyl Transfer Reaction [vSET·AdoMet·Lys27-NH_2 → vSET·AdoHcy·Lys27-N(Me)H_2^+]

Water Channel Allows Proton Dissociation and Formation of the Neutral Amine Lys27-NH_2. Throughout the 4 ns MD simulations, a water channel is positioned to allow the transfer of a proton from Lys27-NH_3^+ to the water solvent. The presence of AdoMet is required for the formation of a water channel. The water molecules forming a water channel are listed in Table 3. The average occupancies (Table 3) of the water bridge from hydrogen bonding analysis on the MD simulations confirm the presence of a water channel.

Lys-NH_3^+ is hydrogen bonded to the first water molecule (Wat914) of the water channel, and when a hydroxide ion is positioned at the solvent end of the water channel, there is no barrier to the transfer of a proton from Lys27-NH_3^+ to HO^- at the QM/MM level [QM = both SCCDFTB and HF/6-31+G(d,p)]. Examination of the environment around the water channel shows that there is no general base candidate.

Free Energy Profile for the First Methyl Transfer Step Catalyzed by vSET. The structure of the reactant is shown in Figure 1. In this structure, the substrate has been formed by loss of a proton from Lys27-NH_3^+. In the structure of the ground state (Figure 1), the N_ϵ(Lys27)−C_γ(AdoMet) and C_γ(AdoMet)−S_δ(AdoMet) bond lengths are 3.17 ± 0.20 and 1.80 ± 0.01 Å, respectively. These key geometric parameters are in agreement with those obtained by Hu et al. at the B3LYP/6-31G*//MM level for the methyl transfer reaction catalyzed by monomethyltransferase SET7/9 (*25*). The calculated average potential energy barrier for the first methyl transfer reaction ($\Delta E^{\ddagger}$) is 21.0 ± 3.7 kcal/mol. Normal mode analysis characterizes the transition state of the monomethylation step (TS-M) with only one imaginary frequency of

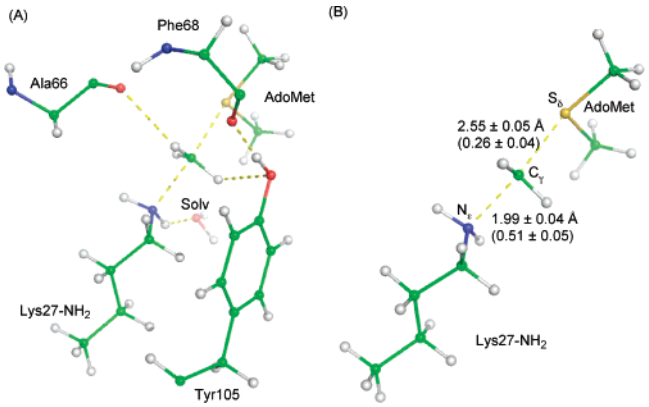

FIGURE 2: Structure of the transition state (TS-M) (A) and close-up of the QM region (B) in the first methyl transfer reaction vSET·AdoMet·Lys-NH_2 → vSET·AdoHcy·Lys-N(Me)H_2^+. The numbers in parentheses are the Wiberg bond orders of the C_γ(AdoMet)−S_δ(AdoMet) and C_γ(AdoMet)−N_ϵ(Lys27) bonds at the TS-M.

321 ± 100i cm^{-1}. In the TS-M (Figure 2), the C_γ(AdoMet)−S_δ(AdoMet) and N_ϵ(Lys27)−C_γ(AdoMet) bond lengths are 2.55 ± 0.05 and 1.99 ± 0.04 Å, respectively, and the N_ϵ-(Lys27)−C_γ(AdoMet)−S_δ(AdoMet) bond angle is 165 ± 5°. This linear configuration at the transition state is in agreement with the requirement of the methylation reactions (*48*). The Wiberg bond orders analysis (Figure 2B) of the N_ϵ(Lys27)−C_γ(AdoMet) and C_γ(AdoMet)−S_δ(AdoMet) bonds at the TS-M indicates that the first methyl transfer step catalyzed by vSET is characterized as 51% associative and 49% disociative because the associability of a reaction is determined by the bond orders of the bond making (*49*). Hu et al. (*25*) reported that the transition state of the methyl transfer catalyzed by SET7/9 was associated with 70% dissociative character. Also, we analyzed the characterization of the transition state of the first methylation catalyzed by "dimer" SET7/9 at the SCCDFTB/MM level. The results show that the transition state of the monomethylation catalyzed by dimer SET7/9 is characterized as being 77 ± 3% dissociative of the bonding making. As compared with the characterization (67 ± 3 and 70 ± 1%) of the transition state catalyzed by monomer SET7/9 (Table 1), there seems to be no significant difference for the characterization of the transition states catalyzed by monomer and "dimer" SET7/9. Thus, the configurations of enzymes have no significant influence on the nature of their transition states. Both enzymatic reactions are linear S_N2 displacements. The vSET reaction is characterized by the Cγ(AdoMet)−N_ζ(Lys27) bond making being ~50% dissociative. The SET7/9 reaction is characterized by the Cγ(AdoMet)−N_ϵ(Lys4) bond making being ~70% dissociative. In both enzymes, there are eight amino acids residues forming the target lysine access channel. Three amino acids are different between the two enzymes. This difference may be the reason for the smaller differences in the structures of the transition states. Perturbation analysis (ref *25* and Table 4) shows that Asn265 in SET7/9 makes a significant and unfavorable contribution to the monomethylation reaction, while the other residues in both vSET and SET7/9 have very smaller influences.

The average contributions of $\Delta(ZPE)^\ddagger$ (0.5 ± 0.9 kcal/mol), $-T\Delta S^\ddagger$ (1.7 ± 0.7 kcal/mol), and $\Delta E_{vib}{}^\ddagger$ (−0.6 ± 0.3 kcal/mol) to the reaction barrier of the first methyl transfer reaction were provided by normal mode analysis. The average free energy barrier to the first methyl transfer reaction is $\Delta G^\ddagger = \Delta E^\ddagger + \Delta(ZPE)^\ddagger - T\Delta S^\ddagger + \Delta E_{vib}{}^\ddagger = 21.0 + 0.5 + 1.7 - 0.6 = 22.5$ kcal/mol and is in excellent agreement with the free energy barrier (21.7 kcal/mol) calculated from the experimental rate constant (0.047 min^{-1}) (*18*). The deviation of $\Delta G^\ddagger$ is ±4.3 kcal/mol. As compared with the calculated free energy (30.9 ± 0.2 kcal/mol) (*50*) of the corresponding methyl transfer reaction in aqueous solution, this enzyme reduces the barrier by 8.4 kcal/mol for the first methyl transfer step. This indicates that the enzyme enhances this methyl transfer reaction by ~10^6-fold.

Table 4: Results of Perturbation Analysis for the Contributions ($\Delta\Delta E^\ddagger$ in kilocalories per mole) of Protein Residues to the Potential Energy Barrier for the First Methylation Step[a]

residue name	residue number	R (Å)	$\Delta\Delta E^\ddagger$
Asp	49	5.7	−3.8 ± 1.6
Arg	54	17.9	−2.2 ± 0.3
Glu	48	9.5	−2.2 ± 1.7
Arg	77	14.8	−2.1 ± 0.3
Arg	26[b]	11.3	−1.9 ± 1.4
Lys	23[b]	21.0	−1.9 ± 1.4
Lys	55	20.4	−1.9 ± 0.3
Arg	77[c]	29.4	−1.6 ± 3.2
Glu	100	14.2	−1.6 ± 0.5
Lys	85	19.6	−1.3 ± 0.1
Arg	88	18.1	−1.0 ± 0.3
Arg	86	18.9	−1.0 ± 0.1
Arg	38[c]	14.5	0.9 ± 0.6
Lys	9	13.8	1.1 ± 0.6
Gly	33[d]	27.4	1.3 ± 3.0
Arg	86[c]	17.8	1.6 ± 0.7
Asp	107	14.9	1.8 ± 0.6
Gly	33[b]	19.7	1.9 ± 0.3
Glu	79	17.9	2.0 ± 0.2
Lys	85[c]	16.3	2.0 ± 0.4
Arg	115[c]	39.5	2.2 ± 3.6
Asp	108	12.5	2.4 ± 0.7
Lys	10	14.2	2.5 ± 1.4

[a] The positive values indicate the favorable contributions that lower the barrier, and the negative values indicate the unfavorable contributions that increase the barrier. R is the distance from the α-carbon of the residue to the center of the water sphere with a 25 Å radius. [b] The residues are located at the substrate. [c] The residues come from the adjacent protein subunit. [d] The residues are from the peptide binding with the adjacent protein subunit.

The first methyl transfer reaction is calculated to be exergonic overall: $\Delta G^\circ = \Delta E^\circ + \Delta(ZPE)^\circ - T\Delta S^\circ + \Delta E_{vib}{}^\circ = -11.5 + 3.1 + 0.2 - 0.2 = -8.8$ kcal/mol. The deviations in ΔG°, ΔE°, $\Delta(ZPE)^\circ$, $T\Delta S^\circ$, and $\Delta E_{vib}{}^\circ$ are ±4.5, ±4.8, ±0.9, ±0.5, and ±0.3 kcal/mol, respectively. The structure of the immediate product vSET·AdoHcy·Lys27-N(Me)H_2^+ is shown in Figure 3. The N_ϵ(Me_2Lys27)−C_γ-(AdoHcy)−S_δ(AdoHcy) bond angle is 153 ± 12°, which is favorable for initiation of the second methyl transfer reaction [vSET·AdoMet·Lys27-N(Me)H → vSET·AdoHcy·Lys27-N$(Me)_2H^+$].

Perturbation Analysis (46, 47) of the Contribution from the Electrostatic Interaction. The results (Table 4) of the perturbation analysis (see Materials and Methods) for the first methyl transfer reaction step indicate that the dominant and favorable effects of Lys10, Asp108, Arg115[b], Lys85[b], and Glu79 decrease the activation energy barrier compared with that in solution and in the gas phase model. Superscripts a and b denote the residues from the substrate peptide and the adjacent protein subunit, respectively. These residues

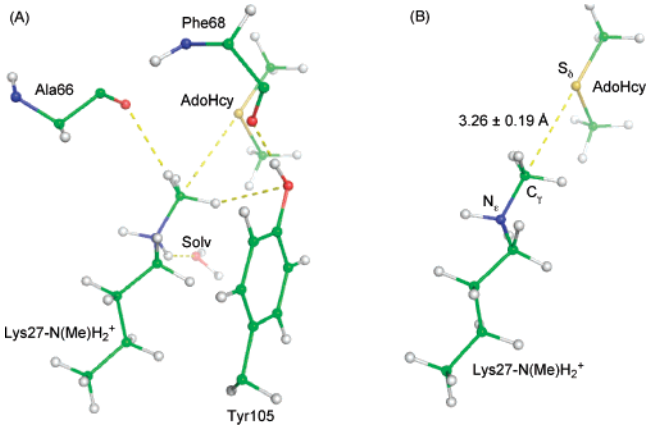

FIGURE 3: Structure of the immediate product vSET·AdoHcy·Lys27-N(Me)H_2^+ (A) and close-up of the QM region (B) in the first methyl transfer reaction vSET·AdoMet·Lys27-NH_2 → vSET·AdoHcy·Lys27-N(Me)H_2^+.

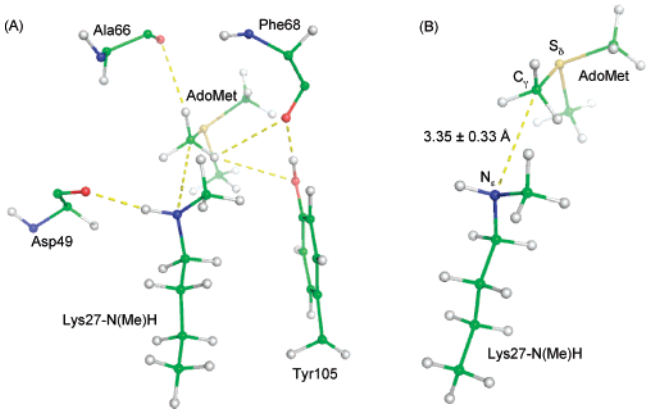

FIGURE 4: Structure of the ground state vSET·AdoMet·Lys27-N(Me)H (A) and close-up of the QM region (B) in the second methyl transfer reaction vSET·AdoMet·Lys27-N(Me)H → vSET·AdoHcy·Lys27-N(Me)$_2$H$^+$.

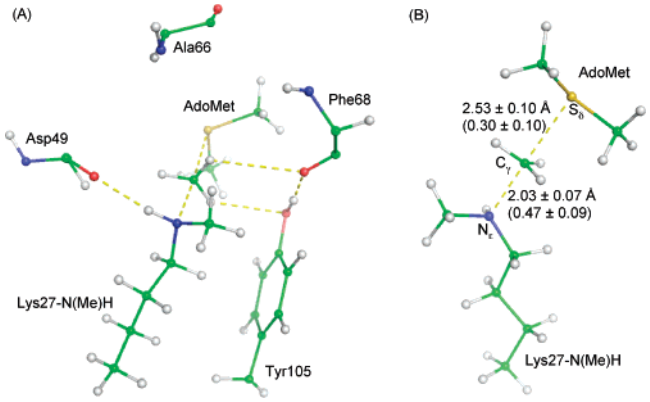

FIGURE 5: Structure of the transition state (TS-D) (A) and close-up of the QM region (B) in the second methyl transfer reaction vSET·AdoMet·Lys27-N(Me)H → vSET·AdoHcy·Lys27-N(Me)$_2$H$^+$. The numbers in parentheses are the Wiberg bond orders of the C_γ(AdoMet)−S_δ(AdoMet) and C_γ(AdoMet)−N_ϵ(MeLys27) bonds at the TS-D.

stabilize the transition state. The residues with unfavorable and dominant contributions to the reaction barrier, including Asp49, Arg54, Glu48, and Arg77, stabilize the reactant state.

The Second Methyl Transfer Reaction [vSET·AdoMet·Lys27-N(Me)H → vSET·AdoHcy·Lys27-N(Me)$_2$H$^+$]

Deprotonation of Lys27-N(Me)H_2^+. The MD simulations on the immediate product [vSET·AdoHcy·Lys27-N(Me)H_2^+] of the first methyl transfer reaction fail to show the water channel that allowed dissociation of a proton from Lys27-N(Me)H_2^+ when AdoHcy is present. The MD simulations on vSET·Lys27-N(Me)H_2^+ still do not indicate the formation of a water channel. It is not until AdoMet replaces the spent AdoHcy at the active site that a water channel forms and is present during 4 ns of MD simulations. The average occupancies (Table 3) of hydrogen bonding throughout the MD simulations confirm the presence of a water channel. Thus, it is the AdoMet cofactor that induces formation of the water channel that allows deprotonation of Lys27-N(Me)-H_2^+ to create the substrate for the second methyl transfer reaction.

Free Energy Profile of the Second Methyl Transfer Step Catalyzed by vSET. The structure of the reactant vSET·AdoMet·Lys27-N(Me)H is shown in Figure 4. The N_ϵ-(MeLys27)−C_γ(AdoMet) and C_γ(AdoMet)−S_δ(AdoMet) bond lengths in the reactant for the second methyl transfer reaction are 3.35 ± 0.33 and 1.81 ± 0.00 Å, respectively (Figure 4). The N_ϵ(MeLys27)−C_γ(AdoMet)−S_δ(AdoMet) bond angle is 140 ± 10°. Because of the methyl group, this ground state bond angle is smaller than that of the nonmethylated reactant of the first methyl transfer reaction. The conformation favors an S_N2 methyl transfer reaction. The calculated average potential energy barrier ($\Delta E^\ddagger$) equals 18.7 ± 1.9 kcal/mol. Normal mode analysis shows that the transition state of the dimethylation step (TS-D) has only one imaginary frequency of 236 ± 102i cm^{-1}. The Wiberg bond orders (Figure 5B) of the N_ϵ(MeLys27)−C_γ(AdoMet) and C_γ(AdoMet)−S_δ-(AdoMet) bonds at the TS-D indicate that the second methyl transfer step catalyzed by vSET is characterized as 47% associative and 53% dissociative. In the TS-D (Figure 5), the N_ϵ(MeLys27)−C_γ(AdoMet) and C_γ(AdoMet)−S_δ(AdoMet) bond lengths are 2.03 ± 0.07 and 2.53 ± 0.10 Å, respectively. The N_ϵ(MeLys27)−C_γ(AdoMet)−S_δ(AdoMet) bond angle is 173 ± 5°. This linear concerted transition state is a requirement of the methylation reactions (*49*).

The average contributions of Δ(ZPE)‡ (1.7 ± 1.2 kcal/mol), $-T\Delta S^\ddagger$ (3.4 ± 1.8 kcal/mol), and ΔE_{vib} (−1.1 ± 0.6 kcal/mol) to the reaction barrier of the second methyl transfer reaction were provided by normal mode analysis. The calculated average free energy barrier of the second methyl transfer reaction is $\Delta G^\ddagger = \Delta E^\ddagger + \Delta(\text{ZPE})^\ddagger - T\Delta S^\ddagger + \Delta E_{vib}{}^\ddagger$ = 18.7 + 1.7 + 3.4 − 1.1 = 22.6 kcal/mol, which is in reasonable agreement with the value of 22.4 kcal/mol determined from the experimental rate constant (0.015 min^{-1}) (*18*). The standard error in $\Delta G^\ddagger$ is ±3.6 kcal/mol.

The second methyl transfer reaction is calculated to be exergonic overall: $\Delta G^\circ = \Delta E^\circ + \Delta(\text{ZPE})^\circ - T\Delta S^\circ + \Delta E_{vib}{}^\circ = -17.4 + 4.4 + 3.4 - 1.2 = -10.8$ kcal/mol. The deviations in ΔG°, ΔE°, Δ(ZPE)°, $T\Delta S^\circ$, and $\Delta E_{vib}{}^\circ$ are ±5.1, ±4.3, ±1.3, ±1.2, and ±0.5 kcal/mol, respectively. The structure of the immediate product vSET·AdoHcy·Lys27-N(Me)$_2$H$^+$ is shown in Figure 6. The N_ϵ(MeLys27)−C_γ(AdoMet)−S_δ(AdoMet) bond angle is 158 ± 10°.

Perturbation Analysis (46, 47) of the Contributions from the Electrostatic Interactions. The perturbation analysis (see Materials and Methods) of the second methyl transfer step (Table 5) indicates that the favorable (and dominant) effects of Glu79, Asp108, Asp107, Gly33[a], and Lys85[b] decrease the

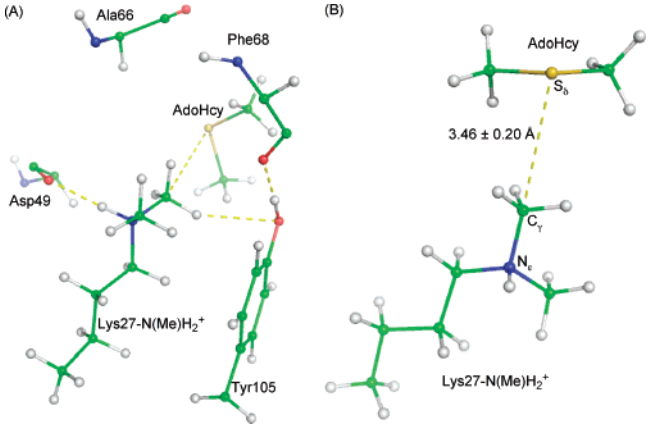

FIGURE 6: Structure of the immediate product vSET·AdoHcy·Lys27-N(Me)$_2$H$^+$ (A) and close-up of the QM region (B) in the second methyl transfer reaction vSET·AdoMet·Lys27-N(Me)H → vSET·AdoHcy·Lys27-N(Me)$_2$H$^+$.

Table 5: Results of Perturbation Analysis for the Contributions ($\Delta\Delta E^‡$ in kilocalories per mole) of Protein Residues to the Potential Energy Barrier for the Second Methylation Step[a]

residue name	residue number	R (Å)	$\Delta\Delta E^‡$
Arg	26[b]	10.7	−3.0 ± 1.3
Glu	100	14.9	−2.6 ± 1.4
Arg	54	16.6	−2.3 ± 0.6
Arg	77	14.7	−2.1 ± 0.8
Lys	55	20.2	−1.7 ± 0.5
Ala	66	3.0	−1.4 ± 2.1
Arg	86	18.8	−1.4 ± 0.6
Lys	85	19.9	−1.3 ± 0.3
Asp	49	3.3	−1.3 ± 3.5
Arg	88	16.0	−1.2 ± 0.4
Phe	68	5.8	−1.1 ± 0.4
Ile	67	5.3	−1.1 ± 0.4
Tyr	50	5.4	−1.1 ± 1.2
Asp	41	19.3	0.9 ± 0.3
Arg	38[c]	16.9	1.1 ± 1.2
Lys	9	14.3	1.1 ± 0.6
Arg	86[c]	17.4	1.3 ± 0.5
Ser	104	11.7	1.3 ± 0.4
Lys	10	14.6	1.6 ± 0.7
Lys	85[c]	16.3	1.9 ± 0.8
Gly	33[b]	23.9	1.9 ± 0.5
Asp	108	17.2	2.1 ± 0.9
Asp	107	16.6	2.1 ± 0.9
Glu	79	15.6	2.1 ± 0.4

[a] The positive values indicate the favorable contributions that lower the barrier, and the negative values indicate the unfavorable contributions that increase the barrier. R is the distance from the α-carbon of the residue to the center of the water sphere with a 25 Å radius. [b] The residues are located at the substrate. [c] The residues come from the adjacent protein subunit.

activation energy, compared with that in solution and in the gas phase model, by stabilizing the transition state. Superscripts a and b denote the residues from the substrate peptide and the adjacent protein subunit, respectively. The unfavorable (and dominant) contributions of Arg26[a], Glu100, Arg54, and Arg77 increase the activation energy; these residues stabilize the ground state.

The Third Methyl Transfer Reaction [vSET·AdoMet·Lys27-N(Me)$_2$ → vSET·AdoHcy·Lys27-N(Me)$_3^+$]

Proton Dissociation of Lys27-N(Me)$_2$H$^+$. The hydrogen bonding analysis, on the MD trajectories on the immediate product vSET·AdoHcy·Lys27-N(Me)$_2$H$^+$, shows that formation of a water channel does not take place. When AdoHcy is released from the active site, the MD simulations on vSET·Lys27-N(Me)$_2$H$^+$ still do not indicate the formation of a water channel. It is not until AdoMet replaces the spent AdoHcy at the active site that a water channel forms and is present during 4 ns of MD simulations. The average occupancies (Table 3) of the water bridge confirm the presence of a water channel. Thus, it is AdoMet that induces formation of the water channel that allows deprotonation of Lys27-N(Me)$_2$H$^+$ and formation of substrate Lys27-N(Me)$_2$ for the third methyl transfer step.

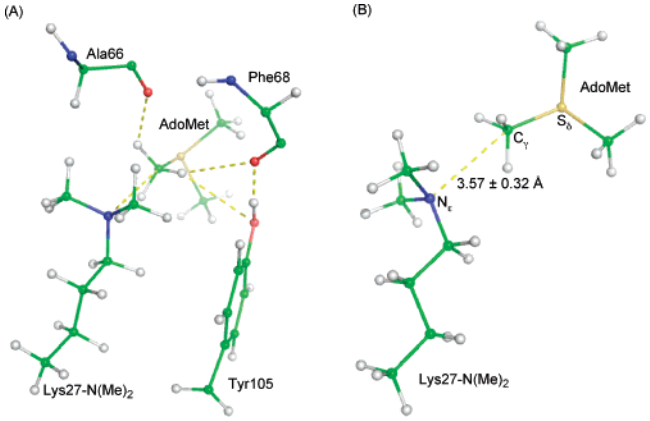

FIGURE 7: Structure of the ground state vSET·AdoMet·Lys27-N(Me)$_2$ (A) and close-up of the QM region (B) in the third methyl transfer reaction vSET·AdoMet·Lys27-N(Me)$_2$ → vSET·AdoHcy·Lys27-N(Me)$_3^+$.

Free Energy Profile of the Third Methyl Transfer Step Catalyzed by vSET. The structure of the reactant is shown in Figure 7. The calculated average free energy is $\Delta G^‡ = \Delta E^‡ + \Delta(\text{ZPE})^‡ - T\Delta S^‡ + \Delta E_{vib}{}^‡ = 20.2 + 0.5 + 3.0 - 0.6 = 23.1$ kcal/mol, which is in reasonable agreement with the value of 23.0 kcal/mol determined from the experimental rate constant (0.005 min^{-1}) (*18*). The standard errors in $\Delta G^‡$, $\Delta E^‡$, $\Delta(\text{ZPE})^‡$, $T\Delta S^‡$, and $\Delta E_{vib}{}^‡$ are ±4.0, ±3.9, ±0.6, ±1.9, and ± 0.6 kcal/mol, respectively. Normal mode analysis shows that the transition state of the trimethylation step (TS-T) has one and only one imaginary frequency of 342 ± 125i cm^{-1}. The Wiberg bond orders (Figure 8B) of the N$_\epsilon$(Me$_2$-Lys27)−C$_\gamma$(AdoMet) and C$_\gamma$(AdoMet)−S$_\delta$(AdoMet) bonds at the TS-T indicate that the third methyl transfer step catalyzed by vSET is characterized as being 41% associative and 59% dissociative. In the TS-T (Figure 8), the N$_\epsilon$(Me$_2$-Lys27)−C$_\gamma$(AdoMet) and C$_\gamma$(AdoMet)−S$_\delta$(AdoMet) bond lengths are 2.08 ± 0.12 and 2.45 ± 0.17 Å, respectively, and the N$_\epsilon$(Me$_2$Lys27)−C$_\gamma$(AdoMet)−S$_\delta$(AdoMet) bond angle is 173 ± 3°. Thus, again the configuration of the transition state is linear and in agreement with a concerted linear transition state (*49*).

The third methyl transfer reaction is calculated to be exergonic overall: $\Delta G^\circ = \Delta E^\circ + \Delta(\text{ZPE})^\circ - T\Delta S^\circ + \Delta E_{vib}{}^\circ = -13.16 + 2.85 + 2.33 - 0.62 = -8.59$ kcal/mol. The standard errors in ΔG°, ΔE°, $\Delta(\text{ZPE})^\circ$, $T\Delta S^\circ$, and $\Delta E_{vib}{}^\circ$ are ±6.09, ±7.47, ±0.93, ±2.30, and ±0.61 kcal/mol, respectively. The structure of the product vSET·AdoHcy·Lys27-N(Me)$_3^+$ is shown in Figure 9. The N$_\epsilon$(Me$_2$Lys27)−C$_\gamma$(AdoHcy)-S$_\delta$(AdoHcy) bond angle is 164 ± 8°. These MD simulations and QM/MM computations support the reaction sequence shown in Scheme 2.

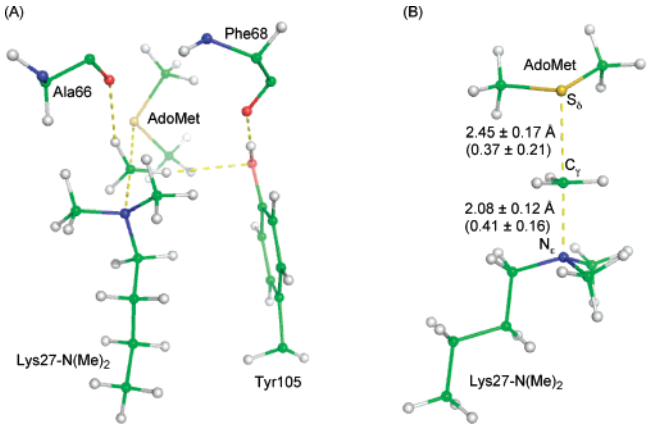

FIGURE 8: Structure of the transition state (TS-T) (A) and close-up of the QM region (B) in the third methyl transfer reaction vSET·AdoMet·Lys27-N(Me)$_2$ → vSET·AdoHcy·Lys27-N(Me)$_3^+$. The numbers in parentheses are the Wiberg bond orders of the C_γ(AdoMet)−S_δ(AdoMet) and C_γ(AdoMet)−N_ϵ(Me$_2$Lys27) bonds at the TS-T.

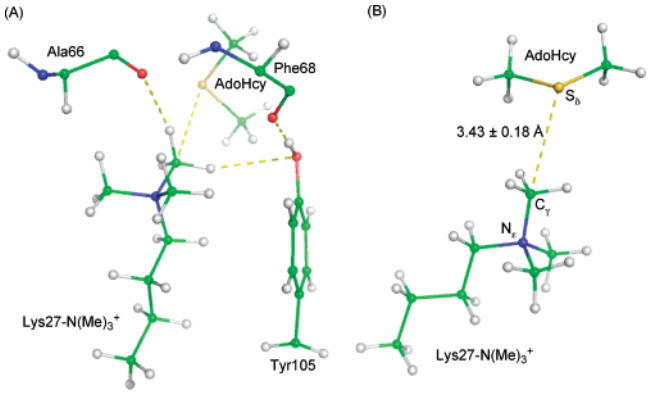

FIGURE 9: Structure of the product vSET·AdoHcy·Lys27-N(Me)$_3^+$ (A) and close-up of the QM region (B) in the third methyl transfer reaction vSET·AdoMet·Lys27-N(Me)$_2$ → vSET·AdoHcy·Lys27-N(Me)$_3^+$.

Perturbation Analysis (46, 47) of the Contributions from the Electrostatic Interactions. The perturbation analysis (see Materials and Methods) for the third methyl transfer step (Table 6) indicates that the favorable (and dominant) effects of Lys85^b, Glu79, Gly33^a, and Asp107 decrease the activation energy compared with that in solution and in the gas phase model; these residues stabilize the transition state. Superscripts a and b denote the residues from the substrate peptide and the adjacent protein subunit, respectively. The unfavorable (and dominant) contributions of Asp49, Arg77, Lys55, Arg26^a, Glu100, and Arg54 increase the activation energy; these residues stabilize the ground state.

Summarizing Perturbation Analysis. All three methylation steps catalyzed by vSET are linear S_N2 reactions with ~50% associative characterizations of the bond making. Perturbation analysis indicates that Gly33^a (the superscript a denotes this residue comes from the peptide substrate), Arg38^b (the superscript b denotes this residue is from the adjacent subunit), Arg85^b, Arg86^b, Glu79, Asp107, and Asp108 stabilize the transition states of all three methylation steps, and Arg26^a, Asp49, Arg54, Lys55, Arg77, Arg86, Arg88, and Glu100 stabilize the ground states of all three methylation steps. Lys9 and Lys10 stabilize the transition states of the first and second methyl transfer steps, but not the third step; Glu48 and Lys85 stabilize the ground state of both the first and third methyl transfer steps, but not the second step. Ile67 and Phe68 stabilize the ground states of the second and third methyl transfer steps, but not the first step.

Scheme 2

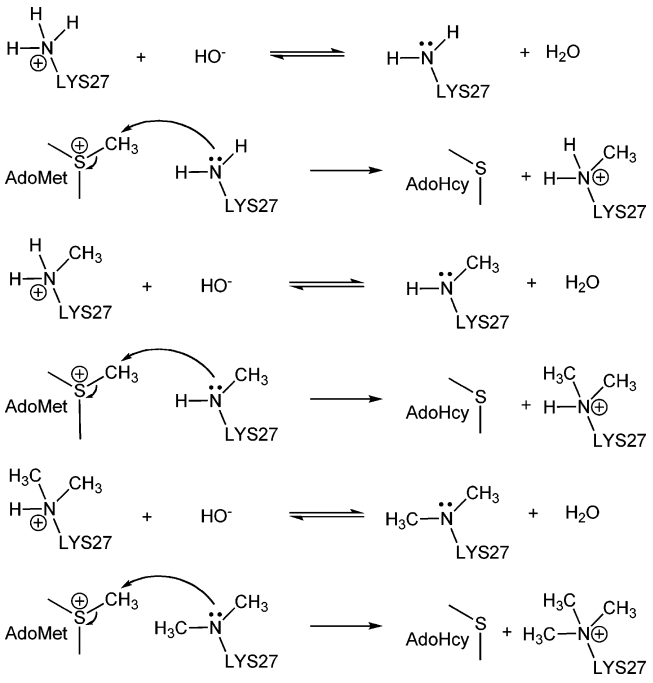

Table 6: Results of Perturbation Analysis for the Contributions ($\Delta\Delta E^\ddagger$ in kilocalories per mole) of Protein Residues to the Potential Energy Barrier for the Third Methylation Step[a]

residue name	residue number	R (Å)	$\Delta\Delta E^\ddagger$
Asp	49	6.7	−4.7 ± 2.6
Arg	77	14.8	−2.7 ± 0.8
Lys	55	22.1	−2.5 ± 1.6
Arg	26[b]	12.0	−2.5 ± 1.2
Glu	100	13.3	−2.0 ± 0.8
Arg	54	18.6	−2.0 ± 0.5
Arg	86	17.7	−1.4 ± 0.5
Ala	66	5.9	−1.4 ± 1.4
Lys	85	19.4	−1.3 ± 0.4
Arg	88	17.0	−1.3 ± 0.4
Glu	48	10.5	−1.2 ± 1.1
Arg	38	19.8	−1.1 ± 0.4
Lys	10[c]	26.2	−1.0 ± 0.7
Phe	68	4.9	−0.9 ± 0.7
Ile	67	3.8	−0.9 ± 0.7
Arg	86[c]	16.3	0.9 ± 0.3
Gly	65	9.2	1.0 ± 0.9
Glu	31	15.8	1.1 ± 0.4

[a] The positive values indicate the favorable contributions that lower the barrier, and the negative values indicate the unfavorable contributions that increase the barrier. R is the distance from the α-carbon of the residue to the center of the water sphere with a 25 Å radius. [b] The residues are located at the substrate. [c] The residues come from the adjacent protein subunit.

CONCLUSIONS

This study establishes the catalytic mechanism and product specificity of viral histone lysine methyltransferase (vSET). Our MD simulations indicate that the formation of a water channel determines if methylation can occur. The water channel appears only in the presence of AdoMet (vSET·Lys27-NH$_3^+$·AdoMet) and is not present in the immediate

products [vSET•Lys27-N(Me)H_2^+•AdoHcy and vSET•Lys27-N(Me)$_2$H$^+$•AdoHcy], vSET•Lys27-N(Me)H_2^+, or vSET•Lys27-N(Me)$_2$H$^+$. Stepwise AdoMet methylation of Lys27-NH_3^+ provides the products Lys27-N(Me)H_2^+, Lys27-N(Me)$_2$H$^+$, and Lys27-N(Me)$_3^+$. Each transfer of a methyl from AdoMet is preceded by proton dissociation to create the neutral amine substrate. Each deprotonation step is preceded by formation of a water channel that allows passage of the proton to solvent water. Our QM/MM calculated free energy barriers for the first, second, and third methyl transfer reactions (Scheme 1) are 22.5 ± 4.3, 22.6 ± 3.6, and 23.1 ± 4.0 kcal/mol, respectively. They are in excellent agreement with the experimental values of 21.7, 22.4, and 23.0 kcal/mol, respectively, determined from the rate constants (0.047, 0.015, and 0.005 min^{-1}, respectively). The Wiberg bond order analysis establishes that the first, second, and third methyl transfer steps catalyzed by vSET are linear S_N2 reactions with the bond making being ~50% associative at the corresponding transition states.

ACKNOWLEDGMENT

Some of the calculations were performed at the National Center for Supercomputing Applications at the University of Illinois (Urbana, IL). We thank the reviewers for valuable comments.

REFERENCES

1. Luger, K. (2004) Structure and dynamic behavior of nucleosomes, *Curr. Opin. Gene Dev. 13*, 127−135.
2. Luger, K., Mader, A. W., Richmond, R. K., Sargent, D. F., and Richmond, T. J. (1997) Crystal structure of the nucleosome core particle at 2.8 Å resolution, *Nature 389*, 251−260.
3. Strahl, B. D., and Allis, C. D. (2000) The language of covalent histone modifications, *Nature 403*, 41−45.
4. Schneider, R., Bannister, A. J., and Kouzarides, T. (2002) Unsafe SETs: Histone methyltransferases and cancer, *Trends Biochem. Biol. 27*, 396−402.
5. Feng, Q., Wang, H., Ng, H. H., Erdjument-Bromage, H., Tempst, P., Struhl, K., and Zhang, Y. (2002) Methylation of H3-lysine 79 is mediated by a new family of HMTases without a SET domain, *Curr. Biol. 12*, 1052−1058.
6. Min, J., Feng, Q., Li, Z. Z., Zhang, Y., and Xu, R. M. (2003) Structure of the catalytic domain of human DOT1L: A non-SET domain nucleosomal histone methyltransferase, *Cell 112*, 711−723.
7. Rea, S., Eisenhaber, F., O'Carroll, D., Strahl, B. D., Sun, Z., Schmid, M., Opravil, S., Mechtler, K., Ponting, C. P., Allis, C. D., and Jenuwein, T. (2000) Regulation of chromatin structure by site-specific histone H3 methyltransferases, *Nature 406*, 593−599.
8. Schultz, J., Milpetz, F., Bork, P., and Ponting, C. P. (1998) SMART, a simple modular architecture research tool: Identification of signaling domains, *Proc. Natl. Acad. Sci. U.S.A. 95*, 5857−5864.
9. Pasini, D., Bracken, A. P., Jensen, M. R., Lazzerini-Denchi, E., and Helin, K. (2004) Suz12 is essential for mouse development and for EZH2 histone methyltransferase activity, *EMBO J. 23*, 4061−4071.
10. Jacobs, S. A., Harp, J. M., Devarakonda, S., Kim, Y., Rastinejad, F., and Khorasanizadeh, S. (2002) The active site of the SET domain is constructed on a knot, *Nat. Struct. Biol. 9*, 833−838.
11. Xiao, B., Jing, C., Wilson, J. R., and Gamblin, S. J. (2003) SET Domain and Histone Metylation, *Curr. Opin. Struct. Biol. 13*, 699−705.
12. Xiao, B., Jing, C., Wilson, J. R., Walker, P. A., Vasisht, N., Kelly, G., Howell, S., Taylor, I. A., Blackburn, G. M., and Gamblin, S. J. (2003) Structure and Catalytic Mechanism of the Human Histone Methyltransferase SET 7/9, *Nature 421*, 652−656.
13. Kwon, T., Chang, J. H., Kwak, E., Lee, C. W., Joachimiak, A., Kim, Y. C., Lee, J., and Cho, Y. (2002) Mechanism of histone lysine methyl transfer revealed by the structure of SET7/9-AdoMet, *EMBO J. 22*, 292−303.
14. Couture, J., Collazo, E., Hauk, G., and Trievel, R. C. (2006) Structural Basis for the Methylation Site Specificity of SET7/9, *Nat. Struct. Biol. 13*, 140−146.
15. Zhang, X., Yang, Z., Khan, S. I., Horton, J. R., Tamarn, H., Selker, E. U., and Cheng, X. (2003) Structural basis for the product specificity of histone lysine methyltransferase, *Mol. Cell 12*, 177−185.
16. Collins, R. E., Techibana, M., Tamaru, H., Smith, K. M., Jia, D., Zhang, X., Selker, E. U., Shinkai, Y., and Cheng, X. (2005) In Vitro and In Vivo Analysis of a Phe/Tyr Switch Controlling Product Specificity of Histone Lysine Methyltransferases, *J. Biol. Chem. 280*, 5563−5570.
17. Min, J., Zhang, X., Cheng, X., Grewal, S. I., and Xu, R. M. (2002) Structure of the SET domain histone lysine methyltransferase Clr4, *Nat. Struct. Biol. 9*, 828−832.
18. Qian, C., Wang, X., Manzur, K., Farooq, S. A., Zeng, L., Wang, R., and Zhou, M. (2006) Structural Insights of the Specificity and Catalysis of a Viral Histone H3 Lysine 27 Methyltransferase, *J. Mol. Biol. 359*, 86−96.
19. Manzur, K. L., Farooq, A., Zeng, L., Plotnikova, O., Koch, A. W., Sachchildanand, and Zhou, M. M. (2003) A dimeric viral SET domain methyltransferase specific to Lys27 of histone H3, *Nat. Struct. Biol. 10*, 187−196.
20. Couture, J., Collazo, E., Brunzelle, J. S., and Trievel, R. C. (2005) Structural and functional analysis of SET8, a histone H4 Lys-20 methyltransferase, *Genes Dev. 19*, 1455−1465.
21. Xiao, B., Jing, C., Kelly, G., Walker, P. A., Muskett, F. W., Frenkiel, T. A., Martin, S. R., Sarma, K., Reinberg, D., Gamblin, S. J., and Wilson, J. R. (2005) Specificity and mechanism of the histone methyltransferase Pr-Set7, *Genes Dev. 19*, 1444−1454.
22. Strahl, B. D., Grant, P. A., Briggs, S. D., Sun, Z. W., Bone, J. R., Caldwell, J. A., Mollah, S., Cook, R. G., Shabanowitz, J., Hunt, D. F., and Allis, C. D. (2002) Set2 is a nucleosomal histone H3-selective methyltransferase that mediates transcriptional repression, *Mol. Cell. Biol. 22*, 1298−1306.
23. Cheng, X., Collins, R. E., and Zhang, X. (2005) Structural and Sequence Motifs of Protein (Histone) Methylation Enzymes, *Annu. Rev. Biophys. Biomol. Struct. 34*, 267−294.
24. Couture, J., Hauk, G., Thompson, M. J., Blackburn, G. M., and Trievel, R. C. (2006) Catalytic Roles for Carbon-Oxygen Hydrogen Bonding in SET Domain Lysine Methyltransferases, *J. Biol. Chem. 281*, 19280−19287.
25. Hu, P., and Zhang, Y. (2006) Catalytic Mechanism and Product Specificity of the Histone Lysine Methyltransferase SET 7/9: An ab initio QM/MM-FE study with Multiple Initial Structures, *J. Am. Chem. Soc. 128*, 1272−1278.
26. Zhang, X. D., and Bruice, T. C. (2007) Catalytic Mechanism and Product Specificity of Rubisco Large Subunit Methyltransferase: QM/MM and MD Investigations, *Biochemistry 46*, 5505−5014.
27. van Etten, J. L. (2003) Unusual life style of giant chlorella viruses, *Annu. Rev. Genet. 37*, 153−195.
28. Jorgensen, W. L., Chandrasekhar, J., Madura, J. D., Impey, R. W., and Klein, K. L. (1983) Comparison of simple potential functions for simulating liquid water, *J. Chem. Phys. 79*, 926−935.
29. Brooks, B. R., Bruccoleri, R. E., Olafson, B. D., States, D. J., Swarminatha, S., and Karplus, M. (1983) CHARMM: A Program for Macromolecular Energy, Minimization, and Dynamics Calculations, *J. Comput. Chem. 4*, 187−217.
30. MacKerell, A. D., Jr., Feig, M., and Brooks, C. L., III (2004) Extending the treatment of backbone energetics in protein force fields: Limitations of gas-phase quantum mechanics in reproducing protein conformational distributions in molecular dynamics simulations, *J. Comput. Chem. 25*, 1400−1415.
31. MacKerell, A. D., Jr., Bashford, D., Bellott, M., Dunbrack, R. L., Jr., Evanseck, J. D., Field, M. J., Fischer, S., Gao, J., Guo, H., Ha, S., Joseph-McCarthy, D., Kuchnir, L., Kuczera, K., Lau, F. T. K., Mattos, C., Michnick, S., Ngo, T., Nguyen, D. T., Prodhom, B., Reiher, W. E., III, Roux, B., Schlenkrich, M., Smith, J. C., Stote, R., Straub, J., Watanabe, M., Wiorkiewicz-Kuczera, J., Yin, D., and Karplus, M. (1998) All-Atom Empirical Potential for Molecular Modeling and Dynamics Studies of Proteins, *J. Phys. Chem. B 102*, 3586−3616.
32. Brunger, A. T., Brooks, C. L., III, and Karplus, M. (1985) Active Site Dynamics of Ribonuclease, *Proc. Natl. Acad. Sci. U.S.A. 82*, 8458−8462.

33. Brooks, C. L., and Karplus, M. (1989) Solvent Effects on Protein Motion and Protein Effects on Solvent Motion: Dynamics of the Active Site Region of Lysozyme, *J. Mol. Biol. 208*, 159−181.
34. Ryckaert, J. P., Ciccotti, G., and Berendsen, H. J. C. (1977) Numerical integration of the Cartesian equations of motion of a system with constraints: Molecular dynamics of n-alkanes, *J. Comput. Phys. 23*, 327−341.
35. Cui, Q., Elstner, M., Kaxiras, E., Frauesheim, Th., and Karplus, M. (2001) A QM/MM Implementation of the Self-Consistent Charge Density Functional Tight Binding (SCC-DFTB) Method, *J. Phys. Chem. B 105*, 569−585.
36. Elstner, M., Porezag, D., Jungnickel, G., Elsner, J., Haugk, M., Frauenheim, Th., Suhai, S., and Seifert, G. (1998) Self-Consistent-Charge Density-Functional Tight-Binding Method for Simulation of Complex Materials Properties, *Phys. Rev. B 58*, 7260−7268.
37. Fischer, S., and Karplus, M. (1992) Conjugate Peak Refinement: An Algorithm for Finding Reaction Paths and Accurate Transition States in Systems with Many Degrees of Freedom, *Chem. Phys. Lett. 194*, 252−261.
38. Wiberg, K. B. (1968) Application of the Pople-Santry-Segal complete neglect of differential overlap method to the cyclopropylcarbinyl and cyclobutyl cation and to bicyclobutane, *Tetrahedron 24*, 1083−1096.
39. Frisch, M. J., Trucks, G. W., Schlegel, H. B., Scuseria, G. E., Robb, M. A., Cheeseman, J. R., Montgomery, J. A., Jr., Vreven, T., Kudin, K. N., Burant, J. C., Millam, J. M., Iyengar, S. S., Tomasi, J., Barone, V., Mennucci, B., Cossi, M., Scalmani, G., Rega, N., Petersson, G. A., Nakatsuji, H., Hada, M., Ehara, M., Toyota, K., Fukuda, R., Hasegawa, J., Ishida, M., Nakajima, T., Honda, Y., Kitao, O., Nakai, H., Klene, M., Li, X., Knox, J. E., Hratchian, H. P., Cross, J. B., Bakken, V., Adamo, C., Jaramillo, J., Gomperts, R., Stratmann, R. E., Yazyev, O., Austin, A. J., Cammi, R., Pomelli, C., Ochterski, J. W., Ayala, P. Y., Morokuma, K., Voth, G. A., Salvador, P., Dannenberg, J. J., Zakrzewski, V. G., Dapprich, S., Daniels, A. D., Strain, M. C., Farkas, O., Malick, D. K., Rabuck, A. D., Raghavachari, K., Foresman, J. B., Ortiz, J. V., Cui, Q., Baboul, A. G., Clifford, S., Cioslowski, J., Stefanov, B. B., Liu, G., Liashenko, A., Piskorz, P., Komaromi, I., Martin, R. L., Fox, D. J., Keith, T., Al-Laham, M. A., Peng, C. Y., Nanayakkara, A., Challacombe, M., Gill, P. M. W., Johnson, B., Chen, W., Wong, M. W., Gonzalez, C., and Pople, J. A. (2004) *Gaussian*, Gaussian, Inc., Wallingford, CT.
40. McQuarrie, D. A. (1973) *Statistical Thermodynamics*, Harper and Row, New York.
41. Zhang, X. D., Swarnalatha, R. Y., and Bruice, T. C. (2007) Mechanism of methanol oxidation by quinoprotein methanol dehydrogenase, *Proc. Natl. Acad. Sci. U.S.A. 104*, 745−749.
42. Zhang, X. D., and Bruice, T. C. (2006) The mechanism of M.HhaI DNA C5 cytosine methyltransferase enzyme: A quantum mechanics molecular mechanics approach, *Proc. Natl. Acad. Sci. U.S.A. 103*, 6148−6153.
43. Zhang, X. D., and Bruice, T. C. (2006) Reaction Mechanism of Guanidinoacetate Methyltransferase Concerted or Stepwise, *Proc. Natl. Acad. Sci. U.S.A. 103*, 16141−16146.
44. Zhang, X. D., Zhang, X. H., and Bruice, T. C. (2005) A definitive mechanism for chorismate mutase, *Biochemistry 44*, 10443−10448.
45. Schmidt, M. W., Baldridge, K. K., Boatz, J. A., Elbert, S. T., Gorden, M. S., Jensen, J. H., Koseki, S., Matsunage, N., Nguyen, K. A., Su, S. J., Windus, T. L., Dupuis, M., and Montgomery, J. A. (1993) General atomic and molecular electronic-structure system, *J. Comput. Chem. 14*, 1347−1363.
46. Cui, Q., and Karplus, M. (2001) Triosephosphate Isomerase: A Theoretical Comparison of Alternative Pathways, *J. Am. Chem. Soc. 123*, 2284−2290.
47. Zhang, X. H., Harrison, D. H. T., and Cui, Q. (2002) The functional specificities of methylglyoxal synthase (MGS) and triosephosphate isomerase (TIM) are not due to stereoelectronic effects: A combined QM/MM analysis, *J. Am. Chem. Soc. 124*, 14871−14878.
48. Coward, J. K. (1977) Chemical mechanisms of methyl transfer reactions: Comparison of methylases with nonenzymic 'model reactions', in *The Biochemistry of Adenosylmethionine* (Salvatore, F., Borek, E., Zappia, V., Williams-Ashman, H. G., and Schlenk, F., Eds.) pp 127−144, Columbia University Press, New York.
49. Takusagawa, F., Fujioba, M., Spies, A., and Schowen, R. L. (1998) S-Adenosylmethionine (AdoMet)-dependent Methyltransferases, in *Comprehensive Biological Catalysis: A Mechanistic Reference* (Sinnott, M., Ed.) pp 1−30, Academic Press, New York.
50. Wang, S., Hu, P., and Zhang, Y. (2007) Ab Initio Quantum mechanical/Molecular Mechanism Molecular Dynamics Simulations of Enzyme Catalysis: The Case of Histone Lysine Methyltransferase SET7/9, *J. Phys. Chem. B 111*, 3758−3764.

BI700515Q